

1 **FULL TITLE: The relative contributions of infectious and mitotic spread to HTLV-**
2 **1 persistence**

3 **SHORT TITLE: Ratio of infectious to mitotic spread in HTLV-1 persistence**

4

5 Daniel J Laydon ^{1,2*}, Vikram Sunkara ³, Lies Boelen ², Charles R M Bangham ^{2*} &
6 Becca Asquith ^{2*}

7

8 ¹ MRC Centre for Global Infectious Disease Analysis, Department of Infectious
9 Disease Epidemiology, School of Public Health, Imperial College London, London W2
10 1PG, United Kingdom;

11 ² Section of Immunology, Wright-Fleming Institute, Imperial College School of
12 Medicine, London W2 1PG, United Kingdom;

13 ³ Department of Mathematics and Computer Science, Freie Universität, Arnimallee 6
14 14195 Berlin, Germany;

15 *Corresponding authors: d.laydon@imperial.ac.uk, c.bangham@imperial.ac.uk,
16 b.asquith@imperial.ac.uk.

17

18 **Abstract (Limit 300 words)**

19 Human T-lymphotropic virus type-1 (HTLV-1) persists within hosts via infectious
20 spread (*de novo* infection) and mitotic spread (infected cell proliferation), creating a
21 population structure of multiple clones (infected cell populations with identical genomic
22 proviral integration sites). The relative contributions of infectious and mitotic spread to
23 HTLV-1 persistence are unknown, and will determine the efficacy of different
24 approaches to treatment.

25 The prevailing view is that infectious spread is negligible in HTLV-1 proviral load
26 maintenance beyond early infection. However, in light of recent high-throughput data
27 on the abundance of HTLV-1 clones, and recent estimates of HTLV-1 clonal diversity
28 that are substantially higher than previously thought (typically between 10^4 and 10^5
29 HTLV-1⁺ T cell clones in the body of an asymptomatic carrier or patient with
30 HAM/TSP), ongoing infectious spread during chronic infection remains possible.

31 We estimate the ratio of infectious to mitotic spread using a hybrid model of
32 deterministic and stochastic processes, fitted to previously published HTLV-1 clonal
33 diversity estimates. We investigate the robustness of our estimates using two
34 alternative methods. We find that, contrary to previous belief, infectious spread
35 persists during chronic infection, even after HTLV-1 proviral load has reached its set
36 point, and we estimate that between 100 and 200 new HTLV-1 clones are created and
37 killed every day. We find broad agreement between all three methods.

38 The risk of HTLV-1-associated malignancy and inflammatory disease is strongly
39 correlated with proviral load, which in turn is correlated with the number of HTLV-1-
40 infected clones, which are created by *de novo* infection. Our results therefore imply
41 that suppression of *de novo* infection may reduce the risk of malignant transformation.

42 **Author Summary (Limits 150-200 words)**

43 There are no effective antiretroviral treatments against Human T-lymphotropic virus
44 type-1 (HTLV-1), which causes a range of inflammatory diseases and the aggressive
45 malignancy Adult T-cell Leukaemia/Lymphoma (ATL) in approximately 10% of
46 infected people. Within hosts the virus spreads via infectious spread (*de novo*
47 infection) and mitotic spread (infected cell division). The relative contributions of each
48 mechanism are unknown, and have major implications for drug development and
49 clinical management of infection. We estimate the ratio of infectious to mitotic spread
50 during the infection's chronic phase using three methods. Each method indicates
51 infectious spread at low but persistent levels after proviral load has reached set point,
52 contrary to the prevailing view that infectious spread features in early infection only.
53 Risk of disease in HTLV-1 infection is known to increase with proviral load, via
54 mutations accrued from repeated infected cell division. Our analyses suggest that
55 ongoing infectious spread may provide an additional mechanism whereby chronic
56 infection becomes malignant. Further, because antiretroviral drugs against Human
57 Immunodeficiency Virus (HIV) inhibit HTLV-1 infectious spread, they may reduce the
58 risk of HTLV-1 malignancy.

59

Introduction

60

61 Human T-lymphotropic virus type-1 (HTLV-1), also known as the human T cell
62 leukaemia virus, infects an estimated 10 million people worldwide [1]. While the
63 majority of infected individuals remain lifelong asymptomatic carriers (ACs), in ~10%
64 the virus causes either Adult T-cell Leukaemia/Lymphoma (ATL) [2] or a range of
65 inflammatory diseases, notably a disease of the central nervous system called HTLV-
66 1-associated myelopathy/tropical spastic paraparesis (HAM/TSP) [3]. HTLV-1 viral
67 burden is quantified by the proviral load (PVL), defined as the number of HTLV-1
68 proviruses per 100 peripheral blood mononuclear cells (PBMCs). During the chronic
69 phase of infection, PVL remains approximately constant [4, 5] within each host, but
70 varies between hosts by over four orders of magnitude; a high PVL is associated with
71 HAM/TSP [5, 6] and ATL [7].

72

73 HTLV-1 replicates in the host through two pathways: mitotic spread and infectious
74 spread [8]. In mitotic spread, an infected cell divides to produce two identical "sister
75 cells" which carry the single-copy provirus integrated in the same genomic location as
76 the parent cell. Infectious spread, or *de novo* infection, occurs when the virus infects
77 a previously uninfected cell, and in this case the virus integrates in a new site in the
78 target cell genome [Figure 1]. The combination of infectious and mitotic spread results
79 in a large number of distinct clones of infected T-cells, each clone defined as a
80 population of infected cells with a shared proviral integration site [9-11].

81

82 The relative contribution of infectious spread and mitotic spread to the proviral load is
83 unknown. This ratio is important, because it will directly determine the efficacy of
84 different approaches to treatment. Although no effective antiretroviral drugs have yet
85 been developed for HTLV-1 infection, antiretroviral therapy (ART), which efficiently
86 reduces infectious spread in HIV-1 infection by inhibiting reverse transcription, viral
87 maturation and proviral integration, may be effective in HTLV-1 infection if infectious
88 spread contributes to the maintenance of HTLV-1 proviral load. Alternatively,
89 immunosuppressive drugs such as ciclosporin which inhibit T cell proliferation would
90 be expected to be more useful if mitotic spread [8] is the dominant mode of viral
91 spread.

92

93 The number of clones of HTLV-1-infected T cells depends on the extent of infectious
94 spread. In this paper, we refer to this number as the HTLV-1 clonal "diversity" (this
95 term should not be confused with measures such as Shannon entropy or beta
96 diversity). The diversity in one host is unknown, and estimating this number from blood
97 samples is nontrivial. Diversity estimation is challenging given the nature of the HTLV-
98 1 clone frequency distribution, where the majority of infected cells are contained in
99 relatively few clones, and the majority of clones contain relatively few cells.

100

101 The prevailing view is that mitotic spread accounts for the majority of HTLV-1
102 persistence [11-14], and that infectious spread is negligible after initial infection [12,
103 13]. This belief is supported by three main observations. First, it was thought that there
104 were relatively few (~100) HTLV-1 clones in one host [9, 11, 13, 15-19]. Second,
105 HTLV-1 varies little in sequence both within and between hosts [20]. Since the host

106 DNA polymerase used in cell proliferation (mitotic spread) is much less error-prone
107 than the viral reverse transcriptase used in infectious spread, a lack of sequence
108 variation implies that infectious spread is rare. Third, many HTLV-1+ clones have been
109 observed at multiple time points separated by several years [9, 17], and a long-lived
110 clone is very unlikely to be maintained by repeated proviral integration through
111 infectious spread at the same integration site, especially since there are no hotspots
112 of HTLV-1 integration [9].

113

114 However, these three observations do not necessarily imply that infectious spread is
115 negligible [14], particularly when we consider the total number of clones in the host
116 and the very small proportion of clones that can be sampled. First, estimates of the
117 number of clones have increased over time [9, 11, 13, 15, 17, 19], and current
118 estimates give approximately 10^4 - 10^5 clones in the circulation of ACs and patients
119 with HAM/TSP [10, 21, 22]. Second, apparent sequence uniformity may result from
120 repeated detection of sister cells from a small number of expanded clones. That is,
121 because of the limitations of sampling, there is a strong bias to detection of the large
122 clones which expanded through mitosis. Finally, the repeated observation of specific
123 clones over many years does not rule out persistent infectious spread. The
124 observation of a temporary but dramatic PVL reduction in a patient with HAM/TSP
125 following treatment with the reverse transcriptase inhibitor lamivudine [23] implies that
126 infectious spread remains important in HTLV-1 persistence, at least in some cases.

127

128 Even when taking recent estimates of clonal diversity into account, there is still good
129 reason to believe that mitotic spread is predominant, because the 10^4 to 10^5 clones

130 (created by infectious spread) present in one host consist of approximately 10^{11}
131 infected cells (maintained by mitotic spread). However, this consideration ignores the
132 possibility that clones may be continuously created by infectious spread and killed by
133 the immune response and natural death.

134

135 The aim of this study was to quantify the rate of infectious spread, and thus the ratio
136 of infectious spread to mitotic spread during chronic infection. We first estimated
137 HTLV-1 clonal diversity in 11 subjects using our previously developed method [10].
138 We next developed a deterministic and stochastic hybrid model of within-host HTLV-
139 1 persistence that we fitted to clonal diversity estimates. We further used two
140 alternative approaches to quantify the rate and to ensure robustness of our estimates.
141 First, we developed a simplified model to approximate the upper bound of the rate.
142 Second, we adapted a method originally developed to model naïve T cell dynamics.
143 We find broad agreement between estimates from all methods. We conclude that,
144 during chronic infection, a given HTLV-1-infected cell in the peripheral blood is
145 substantially more likely to be derived by mitosis of an existing clone than by de novo
146 infection, although infectious spread continues throughout chronic infection with an
147 average of 175 new clones created every day.

148

Methods

149 **Data sets**

150 We apply all three methods described below to previously obtained high-throughput
151 data on HTLV-1 clonality [9]. Each HTLV-1 dataset quantifies the abundance of HTLV-
152 1-infected T cell clones in ex vivo peripheral blood mononuclear cells, without selection
153 or culture. We studied 11 subjects, where each subject had three blood samples taken
154 per time point, at three time points separated by an average of 4 years, giving a total
155 of 99 datasets. All subjects either had HAM/TSP or were asymptomatic carriers of
156 HTLV-1.

157

158 **HTLV-1 clonal diversity estimates**

159 To estimate the rate of infectious spread we first estimated HTLV-1 clonal diversity.
160 We use our recently developed estimator, "DivE" [10, 24, 25], which uses experimental
161 measurements of clonal diversity in a sample to estimate both the number of clones
162 and their frequency distribution in the body of the host [Figure 2A]. DivE fits multiple
163 mathematical models to individual-based rarefaction curves; such curves plot the
164 expected number of clones against the number of infected cells sampled. Numerical
165 criteria score models on their ability to accurately estimate additional data. The best-
166 performing models are extrapolated to estimate the total number of clones in the body,
167 based on the proviral load in each respective subject. See [10, 25] for further details
168 and implementation.

169

170 Table S1 gives the notation used in the three modelling approaches that follow.

171

172 **Modelling approach 1: Full simulation hybrid model**

173 Within a given host, HTLV-1⁺ T cell clones vary in abundance by several orders of
174 magnitude [9, 10]. Broadly, abundant clones can be modelled deterministically but
175 small clones must be modelled stochastically. In the following sections, we describe a
176 model of HTLV-1 dynamics at quasi-equilibrium that is a hybrid of deterministic and
177 stochastic parts [Figure 2].

178

179 Deterministic Model

180 We consider a system with $S(t)$ clones, where a given clone i has frequency $x_i(t)$ at
181 time t . We have the following ordinary differential equations (ODEs) for each clone:

$$182 \quad \frac{dx_i}{dt} = \frac{\pi x_i}{K + N(t)} - \delta x_i \quad (1)$$

183 where $N(t) = \sum_{j=1}^{S(t)} x_j(t)$ is the total number of infected cells summed over all clones at

184 time t ; $\frac{\pi}{K + N(t)}$ is the proliferation rate of infected cells (i.e. the rate of mitotic spread)

185 which is half maximal when $N(t) = K$ (see supplementary information) and δ is the
186 death rate of infected cells [Figure 2B].

187

188 The dynamics of small clones, where random effects are important, will not be
189 adequately described by a deterministic model. Since small clones contain most
190 information about infectious spread, it is important to model these clones accurately,

191 and so we use a discrete stochastic model, in which we consider multiple potential
192 states of each clone and their corresponding probabilities over time.

193

194 Stochastic Model

195 Using a stochastic framework, the number of clones $S(t)$ and their frequencies at time
196 t are considered as random variables, and we describe within-host HTLV-1 dynamics
197 by a set of reactions and their corresponding propensities [supplementary
198 information]. Infected cells can proliferate, die, or infect uninfected cells [Figure 1].

199 Thus the total number of possible reactions $C \in \mathbb{N}$ at time t is $C = 3S(t)$. Following the
200 formulation given in [26, 27], let $X(t) = ((X_i(t))_{i \in S(t)})^T$ be the state vector at time t of all

201 clones. $X(t)$ is a random variable in $\mathbb{N}^{S_{\max}}$ that consists of the random variables

202 $X_i(t) \in \mathbb{N}_0 = \mathbb{N} \cup \{0\}$ of the frequencies $x_i(t)$ of clones $i = 1, \dots, S_{\max}$, where S_{\max} is

203 chosen to always be larger than $S(t)$ for all t . The state vector $X(t)$ evolves through a

204 Markov jump process that depends only on the current state $y \in \mathbb{N}_0^{S_{\max}}$, and its evolution

205 is given by

$$206 \quad X(t) = y_0 + \sum_{c=1}^C P_c \left(\int_0^t \alpha_c(X(s)) ds \right) v_c \quad (2)$$

207 where v_c and α_c respectively denote the stoichiometric vector and propensity function

208 of reaction c [26, 27]. Equation (2) states that the population $X(t)$ at time t is equal to

209 the initial population y_0 plus the sum of the changes induced by all reactions. See

210 supplementary information for further details.

211

212 There exists a probability distribution associated with the random variable $X(t) \in \mathbb{N}_0^{S_{\max}}$
 213 in (2), given by $\mathbb{P}(X;t) = \mathbb{P}(X(t) = y | X(0) = y_0)$, where $y, y_0 \in \mathbb{N}_0^{S_{\max}}$. $\mathbb{P}(X;t)$ is a column
 214 vector where each entry is a probability associated with a potential state of the random
 215 variable at time t . It can be shown [27-30] that $\mathbb{P}(X;t)$ is a solution of the Chemical
 216 Master Equation (CME)

$$217 \quad \frac{\partial \mathbb{P}(X = y;t)}{\partial t} = \sum_{c=1}^C (\alpha_c(y - v_c) \mathbb{P}(X = y - v_c;t) - \alpha_c(x) \mathbb{P}(X = y;t)) \quad (3)$$

218 which describes the rate of change in the probability distribution associated with $X(t)$.
 219 The first term is the sum over all reactions of the probability of arriving at state $X(t) =$
 220 y from state $X(t) = y - v_c$ via reaction c , and the second term is the sum over all
 221 reactions of the probability of leaving state $X(t) = y$ via reaction c .

222

223 For a single clone \mathcal{X}_i , the following reactions respectively describe mitotic spread, cell
 224 death and infectious spread:



228 where

$$229 \quad \pi^*(t) = \frac{\pi}{K + N(t)} \quad (7)$$

230 is the aggregate density-dependent proliferation rate (dependent on the carrying
231 capacity, and the numbers of infected and uninfected cells). The first two reactions of
232 each clone describe a birth-death process, and the lack of inflow from source (i.e. the
233 lack of a reaction $\rho : * \rightarrow \mathcal{X}_i$) defines an absorbing state [Figure 3].

234

235 The reactions (4), (5) and (6) are monomolecular (in terms of the chemical master
236 equation), because they carry the simplifying assumption that cell death due to the
237 host immune response, and the proviral load, are each constant in the equilibrium
238 within each host. HTLV-1 proviral load remains stable over many years [4, 5]: that is,
239 the numbers of infected and uninfected cells stays approximately constant during the
240 chronic phase of infection.

241

242 Simplifying approximations of stochastic model

243 The probability distribution $\mathbb{P}(X;t)$ describes the states and associated probabilities
244 of the entire system, and we define the probability distribution of a particular clone i
245 $\mathbb{P}(X_i;t)$ associated with the random variable $X_i(t)$ similarly:
246 $\mathbb{P}(X_i;t) = \mathbb{P}(X_i(t) = x_i | X_i(0) = x_{i,0})$, where $x_i, x_{i,0} \in \mathbb{N}_0$. The extinction probability of
247 clone i at time t , $\mathbb{P}(X_i = 0;t)$, will be used below to calculate the expected number of
248 clones at time t [Figure 2C], which in turn will enable our model to be fitted to HTLV-1
249 clonal diversity estimates [Figure 2D].

250

251 If clones interact and are modelled with a single master equation associated with
252 $\mathbb{P}(X;t)$, the complexity and runtime of the model increase exponentially with the

253 number of clones. However, because we model the system when proviral load is in
254 equilibrium and can therefore use monomolecular reactions, density-dependent
255 proliferation rates remain approximately constant, and so we can model each clone in
256 isolation with multiple master equations associated with multiple clone-specific
257 distributions $\mathbb{P}(X_i;t)$ ($i = 1, \dots, S(t)$) [Figure 2B]. Therefore, the model complexity and
258 runtime increase only linearly with the number of clones.

259

260 If we impose a maximum frequency for a particular clone i (supplementary information)
261 [Figure 3B], we can summarise Equation (3) using multiple, simpler differential
262 equations below

$$263 \quad \frac{d\mathbb{P}(X_i;t)}{dt} = A\mathbb{P}(X_i;t) \quad \text{for } i = 1, \dots, S_{max} \quad (8)$$

264 where A is the transition matrix or “matrix of connections” [supplementary information]
265 [27, 31, 32]. Further, because the proliferation rate is constant at equilibrium, rates are
266 independent of time, and so Equation (8) has solution

$$267 \quad \mathbb{P}(X_i;t) = e^{At}\mathbb{P}_{0,i} \quad (9)$$

268 where $\mathbb{P}_{0,i} = \mathbb{P}(X_i;t=0)$ is the initial probability distribution and e^{At} is the matrix
269 exponential [33]. For equally spaced time steps $(t_n)_{n=0}^N$ of length h , $\mathbb{P}(X_i;t)$ can be
270 calculated recursively

$$271 \quad \mathbb{P}(X_i;t_n) = e^{Ah}\mathbb{P}(X_i;t_{n-1}). \quad (10)$$

272 Example solutions of Equation (9) are shown in Figure 4.

273

274 Expected number of clones

275 We model the expected number of clones $S(t)$ at time t using by adding the total
276 number of clone “births” $b(t)$ over time (that is, the number of infectious spread events),
277 and subtracting the total number of clone extinctions $E(t)$ over time. $b(t)$ is given by

$$278 \quad b(t) = \int_0^t r_l \left[\sum_{j=1}^{b(u)} x_j(u) \right] du, \quad (11)$$

279 where r_l is the per-capita rate of infectious spread, $x_j(t)$ is the expected frequency of
280 the j^{th} clone to be born since $t=0$ (i.e. $x_j(t) = \mathbb{E}[X_j(t)]$), and $b(0) = 0$. $E(t)$ is then given
281 by

$$282 \quad E(t) = \sum_{j=1}^{b(t)} \mathbb{P}(X_j = 0; t) \quad (12)$$

283 Note that $b(t)$ and $E(t)$ are increasing functions since $r_l, x_j(t) \geq 0$, and because a clone
284 frequency of zero is an absorption state for the random variable $X_j(t)$. Taking (11) and
285 (12) together we calculate the number of clones $S(t)$ as

$$286 \quad S(t) = S_0 + b(t) - E(t) \quad (13)$$

287 where S_0 is the number of clones at time zero [Figure 2C].

288

289 Hybrid model fitting and uncertainty

290 It is estimated that there are approximately 10^{11} HTLV-1 infected cells in one host [10],
291 and so it is not computationally feasible to model all clones using our stochastic
292 formulation. Clones above a certain frequency [$F = 460$ cells; supplementary
293 information] are assumed to be adequately described by the expected value from the
294 deterministic ODEs in Eq. (1) [Figure 2B-D]. We thus partition our system of HTLV-1

295 within-host dynamics into a deterministic system of ODEs, and a stochastic system of
296 master equations [Figure 2B]. We propagate these systems alternatively and
297 concurrently using “Strang splitting” [supplementary information] [34]. The
298 deterministic system described in Equation (1) has $S(t)$ ordinary differential equations.
299 Since the $S(t)$ can exceed 10^5 , we group clones into categories based on the order of
300 magnitude of their abundance.

301

302 We model the dynamics of clones in the body, and not only the blood, because this
303 allows us to model clone extinction. If zero cells of a particular clone are observed or
304 estimated in the blood, this does not necessarily imply that the clone is extinct,
305 because cells in that clone could remain in the solid lymphoid tissue, which contains
306 98% of lymphocytes. We model clones in the body as a whole to avoid this difficulty,
307 which necessitates the assumption that the clonal population structure in the blood is
308 representative of the HTLV-1 clonal structure in the whole body.

309

310 We fitted the infectious spread rate r_I as a free parameter, with all other parameters
311 (infected cell proliferation rate, death rate and density dependency) fixed using
312 previous results from the literature and based on each subject’s proviral load [35]
313 [supplementary information]. For each subject sample and parameter update of r_I , the
314 model was run to reach an approximate equilibrium [Figure 2C]. The model was fitted
315 to the estimated clonal diversity of that subject sample, i.e. to determine the value of
316 r_I required to keep the clonal diversity at the observed equilibrium value [Figure 2D].

317

318 The uncertainty in the estimate of r_i , the rate of infectious spread, derives from three
319 sources: error in model choice (both structure and numerical value of fixed
320 parameters), error in clonal diversity estimation, and sampling variation. Classical
321 methods of quantifying fitted parameter uncertainty only reflect the last source of error
322 (i.e. they assume that the model and the data are correct). We address the first
323 difficulty by using three alternative models with different structures and parameters.
324 We address the error in diversity estimation by using alternative clonal diversity inputs
325 from the Chao1 estimator [36], a non-parametric diversity (or species richness)
326 estimator that has been widely used in many fields [37-40]. And we address the issue
327 of sampling variation by investigating the range of estimates provided by the nine
328 hybrid model fits per subject (i.e. one for each of the subject's blood samples); the
329 mean of these estimates is taken as our point estimate.

330

331 The hybrid model was coded in R (version 3.5.0) [41], using the packages "data.table"
332 [42] and "Matrix" [43]. Matrix exponentials were computed using the Padé
333 approximation [44]. The hybrid was fitted using one-dimensional optimisation as
334 described in [45].

335

336 **Modelling approach 2: upper bound approximation**

337 We considered a simplified model of HTLV-1 persistence that does not describe
338 individual clone dynamics. If $S(t)$ and $N(t)$ are the number of clones and number of
339 infected cells respectively at time t , and r_i is the per-capita rate of infectious spread,
340 we have the following differential equation

341
$$S'(t) = r_I N(t) - \delta_S(t) S(t) \tag{14}$$

342 where $\bar{\delta}_S(t)$ is the *clone* death rate at time t . The first term of Equation (14) models the
343 birth of new clones by infectious spread, and the second term models the death of
344 existing clones.

345

346 If $\bar{\delta}$ is the (constant) death rate of infected *cells*, then we have $\bar{\delta}_S(t) \leq \bar{\delta}$, because the
347 number of clones that die cannot exceed the number of cells that die (equality would
348 occur if all clones were singletons i.e. clones that contain only one infected cell). The
349 clone death rate depends on the population structure of infected cells and will vary
350 over time as this population structure changes. For example, a higher proportion of
351 singletons will increase $\bar{\delta}_S(t)$.

352

353 We assume that, in the chronic stage of infection when HTLV-1 proviral load is at
354 equilibrium, the number of clones is also at equilibrium and so we have $N(t) = N$, $S'(t)$
355 $= 0$, and $S(t) = S$. Letting δ_S be the average rate of clone death, we can approximate
356 Equation (14) as

357
$$S'(t) = 0 = r_I N - \delta_S S \tag{15}$$

358
$$\Rightarrow r_I = \frac{\delta_S S}{N} \leq \frac{\delta S}{N} \tag{16}$$

359 and therefore we define the supremum of the rate

360
$$\Rightarrow r_{I, \text{Supremum}} = \frac{\delta S}{N} . \tag{17}$$

361 $r_{I,Supremum}$ will substantially overestimate infectious spread because it applies the
 362 relatively high singleton death rate to all clones (clones with few cells become extinct
 363 more quickly than clones with many cells). To obtain a tighter upper bound we divide
 364 clones into those smaller and larger than an arbitrary size f_{max} and expand the
 365 expression for r_I in Equation (17) to obtain

$$366 \quad r_{I,f_{max}} = \frac{\hat{\delta}_{small} \sum_{f=1}^{f_{max}} n_f + \hat{\delta}_{large} \sum_{f=f_{max}+1}^{\infty} n_f}{N} \quad (18)$$

367 where n_f denotes the number of clones of frequency f , i.e. the "occupancy classes".
 368 The aggregate clone death rate of small clones $\hat{\delta}_{small}$ and of large clones $\hat{\delta}_{large}$ will
 369 comprise a weighted average of the death rate of clones of all sizes within that
 370 category. Because the HTLV-1 clonal frequency distribution is heavy tailed, small
 371 clones are more numerous than large clones, and so will make the dominant
 372 contribution to the clone death rate. Therefore the contribution from large clones can
 373 be neglected to give

$$374 \quad r_{I,f_{max}} \approx \frac{\hat{\delta}_{small} \sum_{f=1}^{f_{max}} n_f}{N} \quad (19)$$

375 Provided f_{max} is sufficiently small, then $\hat{\delta}_{small}$ (which is less than or equal to δ) can be
 376 approximated by δ . The error incurred by this approximation decreases as f_{max} is
 377 reduced, and so the infectious spread rate will be best approximated by $r_{I,f_{max}}$ for low
 378 values of f_{max} . Estimates of the ratio of infectious spread to mitotic spread can be
 379 obtained by dividing $r_{I,Supremum}$ and $r_{I,f_{max}}$ by the per-capita rate of mitotic spread $\pi =$
 380 0.0316 [supplementary information] to give

381
$$R_{Supremum} = r_{I,Supremum} / \pi \quad (20)$$

382 and

383
$$R_{f_{max}} = r_{I,f_{max}} / \pi . \quad (21)$$

384

385 **Modelling approach 3: Occupancy class model**

386 Adapting an model of naïve T cell dynamics [46], we model the occupancy classes n_f
387 of HTLV-1 clones [Figure 5]. We assume that the clonal structure is in equilibrium (i.e.
388 that the number of clones in each size class is constant) and that the probabilities of
389 cell proliferation and death are independent of clone size.

390

391 Scaling so there is one event (i.e. de novo infection or mitosis) per cell per unit time
392 we have $I + M = 1$ and $R := I / M$. Therefore

393
$$I = R / (1+R) \quad (22)$$

394 and

395
$$M = 1 / (1+R) \quad (23)$$

396 where I and M are the rates of infectious and mitotic spread (scaled as above), and R
397 is the ratio of infectious to mitotic spread.

398

399 A clone in occupancy class f moves to class $f+1$ by mitosis with probability

400
$$Mfn_f / N = fn_f / N(1+R) \quad (24)$$

401 where N is the number of infected cells. A clone in occupancy class $f+1$ moves down
402 to class f by death. Loss of cells by death is equal to the production of new cells by
403 infection and mitosis, which has been scaled to 1, so the death rate is 1 per unit time.

404 Since we assume that the probability of death is independent of clone size, the
 405 probability that the one death event in unit time occurs to a cell in size class $i+1$ is
 406 simply equal to the proportion of cells in size class $i+1$ i.e. fn_i/N .

407

408 In order for the number of cells C_f in size class f ($C_f = fn_f$) to remain constant we require
 409 that flow in and flow out of the occupancy class n_f to be equal [Figure 5], i.e. that the
 410 number of cells leaving occupancy class n_f must be equal to those arriving from class
 411 n_{f-1} (via mitosis) and class n_{f+1} (via cell death). We therefore have

$$412 \quad \frac{1}{1+R} \frac{C_{f-1}}{N} + \frac{C_{f+1}}{N} = \frac{1}{1+R} \frac{C_f}{N} + \frac{C_f}{N} \quad \text{for } f = 2, \dots, \infty \quad (25)$$

413 Rearranging gives

$$414 \quad C_{f+1} = \left(\frac{1}{1+R} + 1 \right) C_f - \frac{1}{1+R} C_{f-1} \quad (26)$$

415 For the number of cells (C_1) in size class 1 to remain constant we require

$$416 \quad \frac{R}{1+R} + \frac{C_2}{N} = \frac{1}{1+R} \frac{C_1}{N} + \frac{C_1}{N} \quad (27)$$

417 And for the population as a whole to remain of constant size we need the gain of new
 418 clones to balance their loss

$$419 \quad \frac{R}{1+R} = \frac{C_1}{N} \quad (28)$$

420 Rearranging (28) gives our first estimator (R_1) for the ratio R from the occupancy class
 421 model, given in terms of $p = C_1/N$, the proportion of cells that are singletons:

$$422 \quad R = \frac{p}{1-p} \quad (29)$$

423 Substituting (28) into (27) and applying (26) recursively we obtain

$$424 \quad C_f = \frac{1}{1+R} C_{f-1} \quad \text{for } f = 2, 3, \dots, \infty \quad (30)$$

425 and thus

$$426 \quad C_f = \left(\frac{1}{1+R} \right)^{f-1} N \frac{R}{1+R}. \quad (31)$$

427 Species richness is defined as the number of clones, and so

$$\begin{aligned} \text{Species richness} &= \sum_{f=1}^{\infty} n_f \\ 428 \quad &= \sum_{f=1}^{\infty} \frac{C_f}{f} \quad (32) \\ &= \sum_{f=1}^{\infty} \left(\frac{1}{1+R} \right)^{f-1} \frac{N}{f} \frac{R}{1+R} \end{aligned}$$

429 obtained by substituting in (31).

430

431 Using the fact that $\sum_{k=1}^{\infty} \frac{z^k}{k} = \ln \left(\frac{1}{1-z} \right)$ (a special case of the polylogarithm function)

432 We have that

$$433 \quad \text{species richness} = \ln \left(\frac{1+R}{R} \right) NR \quad (33)$$

434 This is our second estimator for the ratio of infectious to mitotic spread, R_2 , from the
435 occupancy class model.

436

437 The proportion of infected cells that are singletons is estimated using DivE, and the
438 number of infected cells in the body is estimated from each patients proviral load as
439 described in [10].

440

Results

441 HTLV-1 clonal diversity estimates

442 We estimated HTLV-1 clonal diversity (the number of unique clones) in 11 subjects
443 with non-malignant HTLV-1 infection, either asymptomatic carriers or those with
444 HAM/TSP. These estimates were obtained by measuring diversity in the nine blood
445 samples per person (three at each of three time points) and then applying our recently
446 developed method of estimating clonal diversity by extrapolation from the sample to
447 the whole body [10] [Table 1].

448 We tested our assumption that the number of clones is at equilibrium in the chronic
449 phase of infection, where HTLV-1 proviral load is at equilibrium. We used linear
450 regression to estimate the net change per day in the observed and estimated number
451 of clones. This net change was 0.01 (95% CI -0.07 – 0.09) clones per day (i.e. 1 clone
452 every 100 days) and -2.50 (-5.94 – 0.93) clones per day in the observed and estimated
453 number of clones respectively; in each case the confidence interval spans zero.
454 Further, using a two-tailed binomial test, we found little evidence that this change was
455 significantly different from zero ($p = 1$ for observed and $p = 0.07$ for estimated). We
456 therefore make the approximation that HTLV-1 clonal diversity remains unchanged in
457 the chronic phase of infection, after the proviral load has reached steady state.

458

459 Modelling approach 1: Full simulation hybrid model

460 Within-host HTLV-1 persistence is modelled by considering HTLV-1-infected clones
461 individually. Large clones are modelled deterministically using a system of ordinary
462 differential equations, whereas smaller clones are modelled stochastically by solving

463 the chemical master equation [Equations (9) and (10)] that considers the frequency of
464 each clone as a random variable governed by a birth-death process [Figure 2B]. The
465 per-capita rate of infectious spread and the expected number of infected cells are then
466 combined to model the birth of new clones (11), whereas the extinction probability of
467 each clone is used to calculate expected clone death (12). The birth and death (or
468 extinction) of clones provide an estimate of the number of clones at equilibrium (13)
469 [Figure 2C], and it is this value that is fitted to our estimates of HTLV-1 clonal diversity,
470 to infer the per-capita rate of infectious spread [Figure 2D].

471

472 The hybrid model was fitted to clonal diversity estimates for each subject (for each
473 sample and each time point), providing an estimate of the infectious spread rate in
474 each case [Table 1]. These nine estimates per patient were averaged to calculate the
475 mean rate for each individual. Between individuals, the mean estimated rate of
476 infectious spread was 7.7×10^{-10} per day, ranging from 2.1×10^{-10} to 1.7×10^{-9} per
477 day [Figure 6A], i.e. varying by almost an order of magnitude. While this per-capita
478 rate is very low, it translates to an average of 175 (range 39 - 456) new clones created
479 per day [Figure 6B]. Therefore the hybrid model predicts that infectious spread is not
480 limited to initial infection, but persists at a low level throughout the chronic phase.
481 Given an estimate of the rate of mitotic spread of 3.2×10^{-2} per day, our infectious
482 spread estimates imply an average ratio of infectious to mitotic spread of 2.4×10^{-8}
483 ($6.6 \times 10^{-9} - 5.3 \times 10^{-8}$) [Figure 7].

484

485 Within individuals the standard deviation between samples in the infectious spread
486 rate was relatively small, with an average of 2×10^{-10} ($5.4 \times 10^{-11} - 4.1 \times 10^{-10}$) [Table

487 1]. Estimates of the per-capita infectious spread rate were not found to correlate with
488 either proviral load or with the estimated diversity during the chronic phase (this may
489 be due to our 11 patients providing insufficient power). However, unsurprisingly, the
490 estimated number of new clones per day was correlated with both proviral load ($R^2 =$
491 0.62) and strongly correlated with the estimated diversity ($R^2 = 0.99$) [Figure S1].

492

493 Sensitivity analysis of hybrid model

494 Originally our threshold value of F , above and below which clones are respectively
495 modelled deterministically and stochastically, was set to equal 100. However, the
496 extinction probability of clones of size 100 over a duration of $t_{Dur} = 3133$ days
497 [supplementary information] duration was 0.37. We were therefore concerned that
498 excluding such clones would bias the estimates of the infectious spread rate and
499 therefore the ratio, and so re-fitted our model with $F = 460$. This value is the minimum
500 clone frequency for which the extinction probability is less than 1%, given our
501 parameters of infected cell growth, death, and density dependency [Figure S2,
502 supplementary information]. The estimates of infectious spread from the hybrid model
503 are almost identical whether we assume $F = 100$ or $F = 460$. We present the $F = 460$
504 estimates, as the most accurate description of the system would to consider all clones
505 stochastically. The results of a sensitivity analysis on the length of the time step h are
506 shown in Figure S3.

507

508 **Modelling approach 2: upper bound approximation**

509 Upper bounds of the infectious spread rate ($r_{i,Supremum}$) were estimated for each subject
510 using Equation (17), by substituting inputs of HTLV-1 clonal diversity estimates [Table

511 1] and an estimate of $\delta = 0.0316$ infected cell death a day, and an estimate of the total
512 number of infected cells N (derived from the proviral load, as detailed in [10]). For each
513 individual we averaged across all samples and across all time points. Estimated values
514 of the rate ranged between individuals from 2.8×10^{-9} to 1.7×10^{-8} per infected cell
515 per day, and thus (given a rate of per-capita mitotic spread of 0.0316 cells per day)
516 estimates of the ratio $R_{Supremum}$ ranged between 8.7×10^{-8} and 5.5×10^{-7} [Figure 6A].
517 The estimated number of new clones per day using the supremum estimates are
518 unsurprisingly much larger than those of the hybrid, ranging from 516 to 4804, i.e.
519 approximately an order of magnitude higher [Figure 6B].

520

521 We further estimated the more restrictive upper bounds of the ratio $R_{f_{max}}$ from Equation
522 (21) for multiple f_{max} values between 1 and 1000 [Figure 6A]. These estimates assume
523 that the cell death rate applies to clones with frequencies less than or equal to f_{max} ,
524 and that larger clones do not contribute to the rate.

525

526 The hybrid estimates always fall below the estimated supremum and are very close to
527 the estimates provided by for $f_{max} = 1$ [Figure 6]. Since it is likely that the upper bound
528 approximation will give more accurate estimates for lower values of f_{max} , this result
529 demonstrates the consistency of estimates produced between the hybrid and the
530 upper bound approximation.

531

532 **Modelling approach 3: Occupancy class model**

533 The results from the hybrid model indicate a very low ratio of infectious to mitotic
534 spread. The hybrid benefits from treating small clones stochastically and from the
535 inclusion of known experimental details of HTLV-1 infection and spread. However, it
536 remained possible that these very low estimates of the ratio resulted from incorrect
537 model or parameter assumptions. To test the robustness of our estimate of the ratio
538 to changes in model and parameter assumptions, we adapted a simple deterministic
539 model of HTLV-1 clonal dynamics and occupancy classes and used this to produce
540 two alternative estimators of the ratio of infectious to mitotic spread.

541

542 The occupancy class model is based on a model of naïve T cell dynamics developed
543 by de Greef et al [46]. It assumes that clonal dynamics are deterministic, that the clonal
544 structure is in equilibrium and that the probabilities of cell proliferation and death are
545 independent of clone size. The model yields two estimators of the ratio of infectious to
546 mitotic spread. The first estimator (referred to as R_1) depends on the proportion of
547 infected cells that are singletons

548
$$R_1 = \frac{P}{1-p}$$

549 where p is the proportion of cells that are singletons.

550

551 The second estimator (referred to as R_2) depends on species richness.

552
$$\text{species richness} = \ln \left[\frac{1+R_2}{R_2} \right] NR_2$$

553 where N is the number of infected cells (see Methods for derivation of both
554 expressions).

555

556 Across the 99 estimates (11 subjects, 3 time points, 3 replicates) both estimators, R_1
557 and R_2 , are strongly positively correlated with the estimate of the ratio produced by
558 the hybrid model ($P = 1 \times 10^{-135}$ and $P = 6 \times 10^{-87}$ respectively, Pearson correlation)
559 and agree well numerically, being of the same order of magnitude and, if anything
560 tending to be even smaller (hybrid median = 2.0×10^{-8} , hybrid LQ = 1.4×10^{-8} , hybrid
561 UQ = 3.0×10^{-8} ; R_1 median = 2.0×10^{-8} , R_1 LQ = 1.4×10^{-8} , R_1 UQ = 3.0×10^{-8} ; R_2
562 median = 1.3×10^{-8} , R_2 LQ = 1.0×10^{-8} , R_2 UQ = 1.9×10^{-8}) [Figure 8].

563

564 Finally, we applied the second estimator from the occupancy class model to estimate
565 infectious spread (R_2) to the Chao1 estimator of clonal diversity (rather than the DivE
566 estimate used up to this point). The Chao1 estimator gives much lower diversity
567 estimates, and so unsurprisingly yields considerably smaller estimates of the
568 infectious to mitotic spread ratio (median = 7.3×10^{-10} , LQ = 4.7×10^{-10} , UQ = $1.0 \times$
569 10^{-9}).

570

571 We conclude that the low estimates of the infectious to mitotic spread are not the
572 product of implicit assumptions in the hybrid model or incorrect parameter choice.
573 Inaccurate estimates of the clonal diversity may play a significant role but calculations
574 using an alternative, widely used estimator provided even smaller estimates of clonal
575 diversity, and therefore yield an even lower ratio.

576

Discussion

577

578 The relative contribution of infectious and mitotic spread to HTLV-1 viral persistence
579 has not previously been estimated, and this has been a long-standing problem in the
580 field. For many years, it was believed that the virus persisted solely by oligoclonal
581 proliferation of latently infected cells, and that infectious spread contributed little if
582 anything to persistence. However, three observations have brought this belief into
583 question. First, the strong, persistently activated host T-cell response to HTLV-1
584 implied that the virus is not latent but is frequently expressed in vivo. Second, high-
585 throughput analysis revealed that a typical host carries between 10^4 and 10^5 clones,
586 not ~100 clones as was previously believed. Third, treatment with the antiretroviral
587 therapy lamivudine temporarily but substantially reduced the proviral load of a patient
588 with HAM/TSP. These observations raise the question: what is the contribution of
589 infectious spread to the maintenance of the proviral load during chronic infection?

590

591 In this study, we used three different strategies to estimate the ratio of infectious to
592 mitotic spread during the chronic phase of infection. We first developed a deterministic
593 and stochastic hybrid model of within-host HTLV-1 dynamics, and fitted this model to
594 clonal diversity estimates derived from experimental data. We then derived an
595 estimate of the upper bound of the ratio by using a highly simplified model that does
596 not consider individual clones. Finally, we adapted a model of naïve T cell repertoires
597 that models clone occupancy classes. We found broad agreement between the
598 estimates of the ratio obtained using all three methods; and each method implied the

599 existence of ongoing infectious spread during chronic infection, after the HTLV-1
600 proviral load has reached steady state.

601

602 While the ratio of infectious to mitotic spread during the chronic phase is very small
603 ($\sim 2 \times 10^{-8}$), it equates to $\sim 10^2$ new clones every day. That is, approximately 100 new
604 HTLV-1-infected T cell clones appear every day by infectious spread. Further, while
605 the estimated rate of infectious spread represents a small contribution to overall HTLV-
606 1 persistence, the constant creation of new clones will increase the risk of malignant
607 transformation, because this risk depends in part on the proviral integration site [21].
608 A malignant clone could originate not only from accumulated mutations in a long-lived
609 clone, but also from a recently infected clone. High HTLV-1 proviral load increases
610 both clonal diversity [47] and risk of ATL [7]. However, it is unknown whether the
611 increased clonal diversity (caused by infectious spread) is a mechanism for this higher
612 risk of malignancy, or whether it is a separate bi-product of high proviral load. Our
613 estimates of ongoing infectious spread during chronic infection are consistent with the
614 hypothesis that higher infectious spread increases the risk of malignant
615 transformation. If this is the case, then anti-retroviral therapy could reduce the risk of
616 ATL in patients who have entered their chronic phase, although it would need to be
617 continued for many years, and would be a long time before its impact was evident.

618

619 It is important to note that the different methods we use are not independent. First,
620 they all use our clonal diversity estimates as an input (see section below). Second,
621 they all assume equilibrium clonal diversity. However, they do differ in a number of
622 respects. The upper bound approximation is independent of the parameters F , π and

623 K and makes no assumptions about the clonal structure or the density dependence of
624 infected cell proliferation. The R_1 estimator from the occupancy class model depends
625 only on the proportion of singletons and so is independent of all the parameters (F , π ,
626 δ and K), assumptions about density dependence of proliferation, and indeed the
627 estimated clonal structure beyond the number of singletons. Similarly the R_2 estimator
628 from the occupancy class model is also independent of F , π , δ and K as well as
629 proliferation assumptions. While the hybrid model is our most detailed simulation of
630 HTLV-1 within host dynamics, it is mathematically and computationally complex and
631 requires significant runtime. Because the estimates from all three methods are largely
632 consistent, our analysis indicates that the latter two methods provide good
633 approximations of the rate of infectious spread and the ratio of infectious to mitotic
634 spread.

635

636 The most likely source of error in our estimates of the ratio of infectious to mitotic
637 spread lies in the estimation of clonal diversity. Two factors argue against a serious
638 error. First, estimates based on two different quantities (the number of clones and the
639 proportion of infected cells that are singletons) give very similar estimates of the ratio.
640 Second, the DivE estimator compares favourably to other widely-used estimators of
641 species richness [10]. It remains possible that we have underestimated clonal
642 diversity, although it is important to note that DivE produces considerably higher and
643 more plausible estimates than the other estimators, which predicted fewer clones than
644 were observed in additional blood samples taken at the same time.

645

646 A much smaller source of potential error lies in using the number of clones to quantify
647 infectious spread. If the virus repeatedly integrates in the same genomic site, then the
648 number of unique genomic sites would be less than the number of true clones, and
649 hence both the infectious spread rate and the ratio would be underestimated.
650 However, hotspots of HTLV-1 integration have not been observed [9], and so such
651 repeat infection would not substantially alter our estimate. Assuming the provirus does
652 not efficiently integrate into heterochromatin, which represents $\sim 2/3$ of the human
653 genome, then only one third of the $\sim 3 \times 10^9$ base pairs of the human genome have
654 the potential for proviral integration. The probability of repeated proviral integration is
655 then the number of existing integration sites divided by the number of potential
656 integration sites. Given the estimated number of clones is of the order of 10^5 , this
657 probability is approximately $10^5/10^9 = 10^{-4}$. Therefore, any error in using the number
658 of clones to quantify infectious spread is very small.

659

660 It seems surprising that, during initial infection, the virus could establish a stable
661 population of infected T cell clones with such a low rate of infectious spread. However,
662 these low rates of infectious spread are measured in the chronic phase of infection,
663 when the strong host cytotoxic response kills HTLV-1-expressing cells, which probably
664 reduces efficient infectious transmission and favours mitotic transmission. During the
665 early phase of infection, before the establishment of an adaptive immune response,
666 the contribution of infectious spread may be substantially higher than during chronic
667 infection. It would be interesting to model the dynamics of early infection, in particular
668 to investigate the rate required to establish a stable population of infected T cell clones.
669 Modelling early infection would violate the assumption of equilibrium, and thus would
670 void many of the simplifying assumptions that makes our model tractable (e.g. our

671 ability to model clones independently and so avoid an exponential increase in
672 complexity). However, given sufficient computational power, this analysis would be
673 possible.

674

675 The methods described here have potential applications in other fields, for example in
676 modelling the human T cell receptor (TCR) repertoire. The mechanisms by which the
677 immune system is reconstituted after immune suppression or transplantation are
678 poorly understood. Drawing parallels between immune reconstitution and HTLV-1
679 infectious and mitotic spread, the present approach could be applied to investigate the
680 extent to which reconstitution occurs either through the generation of new TCR
681 clonotypes, or through the expansion of existing clonotypes. In HIV-1 infection, the
682 approach could be used to quantify the ratio of infectious to mitotic spread in the
683 absence of treatment and in the latent reservoir remaining following treatment.

684

685 In summary, we develop three methods, which have the potential to be applied to a
686 range of areas, and use them to quantify the role of de novo infection in maintaining
687 HTLV-1 viral burden at equilibrium. We find that on average 5×10^9 new infected cells
688 are produced every day; of these the vast majority (>99.9%) will arise from division of
689 an existing infected cell and will thus have the same proviral integration site as their
690 mother cell, but a small minority (about 175 cells per day) will arise from infectious
691 transmission and will contain a novel proviral integration site. These estimates suggest
692 that ongoing infectious spread may be a mechanism for malignant transformation that
693 treatment with antiretroviral drugs may suppress.

694

695 **Acknowledgements**

696 We acknowledge grant funding from the Bill and Melinda Gates Foundation, joint
697 Centre funding from the UK Medical Research Council and Department for
698 International Development (grant MR/R015600/1), the Wellcome Trust (Project Grant
699 091845 to CB, BA; Senior Investigator Award 100291 to CB), and the Imperial College
700 National Institute for Health Research Biomedical Research Centre. We thank the
701 High Performance Computing service staff at Imperial College
702 (<https://www.imperial.ac.uk/computational-methods/hpc/>), and the staff at the National
703 Centre for Human Retrovirology, Imperial College Healthcare NHS Trust, London,
704 U.K. B.A. is a Wellcome Trust Investigator (103865) and is funded by the Medical
705 Research Council UK (J007439 and G1001052), the European Union Seventh
706 Framework Programme (FP7/2007–2013) under grant agreement 317040 (QuanTI)
707 and Leukemia and Lymphoma Research (15012).

708

Figures

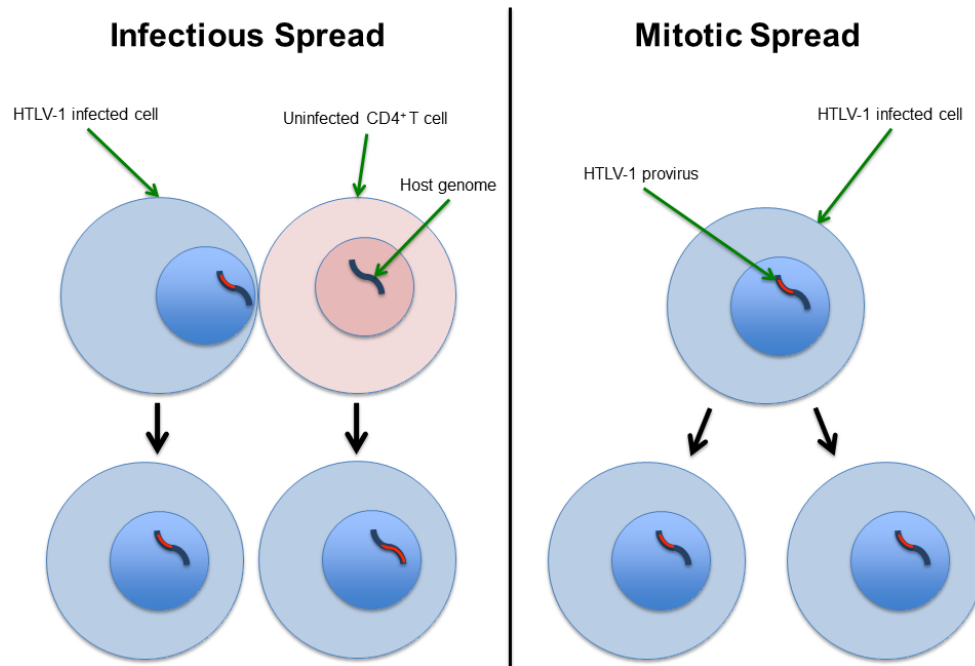


Figure 1. HTLV-1 infectious and mitotic spread schematic. Left column (Infectious spread): an HTLV-1-infected cell infects an uninfected CD4⁺ T cell (typically by cell-to-cell contact via the virological synapse, and potentially also via cell-free spread). The HTLV-1 provirus (red) integrates in a different genomic location in the newly infected cell, so infectious spread has resulted in two clones. Right column (Mitotic spread): An HTLV-1-infected cell divides, whereupon the provirus resides in the same genomic location in each daughter cell. The figure shows a single clone with two HTLV-1-infected cells.

709

710

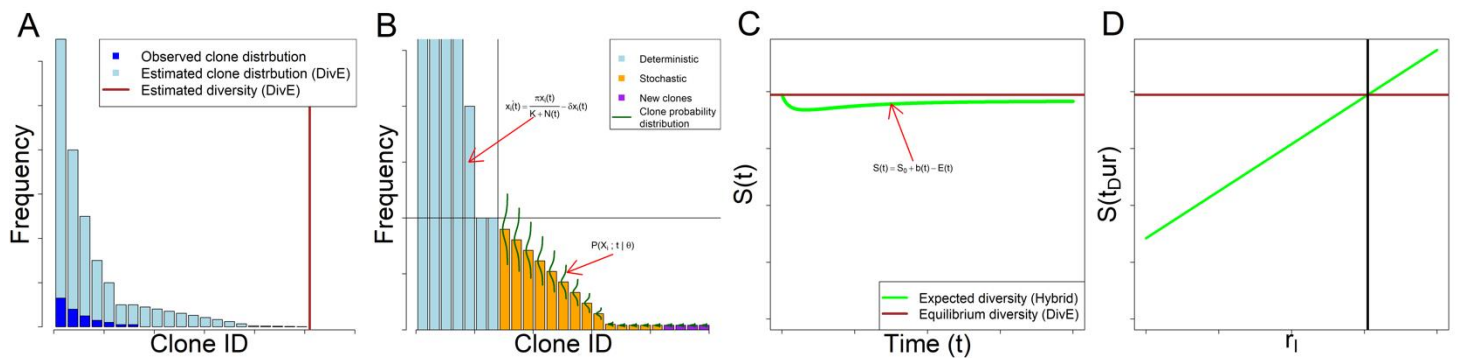
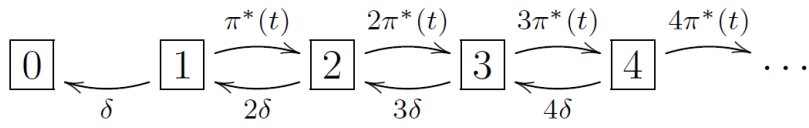


Figure 2: Schematic of full simulation hybrid model. **A:** Observed and estimated clone frequency distributions. From an observed sample of clones, the clone frequency distribution of the body in one host is estimated using DivE. **B:** Propagation of hybrid model: Estimated clone frequency distribution partitioned into deterministic and stochastic systems. Clones of frequency less than and greater than threshold F are respectively modelled stochastically and deterministically. F is chosen with respect to probability of clone extinction [supplementary information]. The deterministic system is modelled using ordinary differential equations [Eq. (1)]. The stochastic system consists of multiple birth-death processes (one for each stochastically modelled clone) each with an absorbing state at zero [Figure 3]. The evolution of the clone probability distribution over time is governed by the chemical master equation [Eq. (10), Figure 4]. New clones are created through infectious spread, i.e. the per-capita rate r_i multiplied by the expected number of infected cells, in both deterministic and stochastic compartments [Eq. (11)]. Deterministic and stochastic systems are propagated concurrently with Strang splitting [supplementary information]. **C:** Hybrid model diversity. The estimated number of clones $S(t)$ [Eq. (13)] at time t , given parameters $\theta = \{\pi, \delta, K, r_i\}$ is given by the number of clones created [Eq. (11)], minus the number of clones that are expected to have died between 0 and t [Eq. (12)], plus the number of clones S_0 at $t = 0$. The number of clones is assumed to be at equilibrium in the chronic phase of infection. **D:** Model fitting schematic: Expected diversity at $S(t_{Dur})$ increases with per-capita infectious spread rate r_i . Model fitted using non-linear least squares to DivE estimated diversity in the body, where the objective function is the square of the discrepancy between this value and the value of $S(t_{Dur})$ at equilibrium.

711

A



B

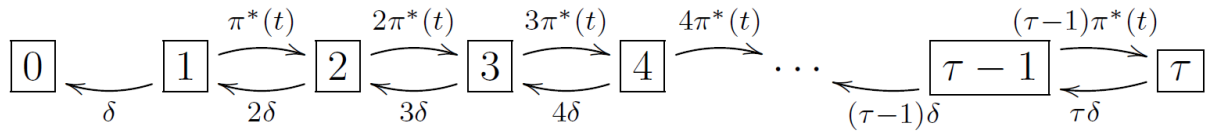
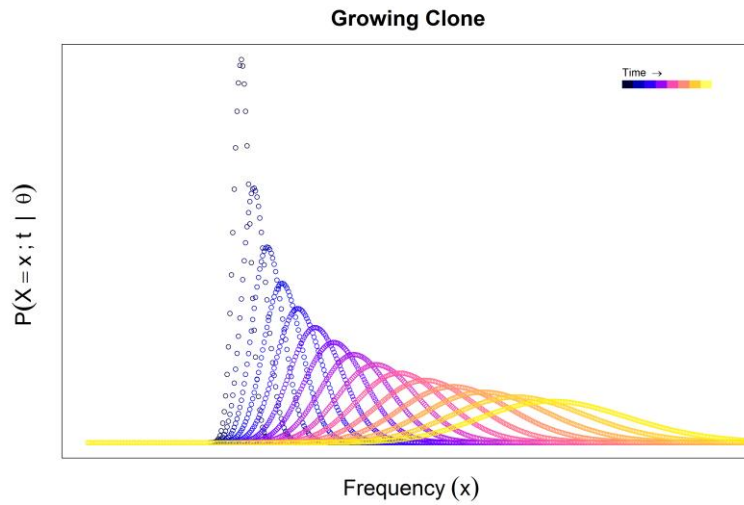


Figure 3. Clone state space birth-death process flow diagram. Each box denotes the potential state of a given clone, i.e. the number of cells in that clone, with the corresponding propensity of each reaction at each state. $\pi^*(t)$ and δ denote the per-capita rates of infected cell proliferation and death respectively. Note there is no source inflow from frequency 0 to frequency 1. **A** and **B** respectively show the state space with and without an upper limit τ .

712

A



B

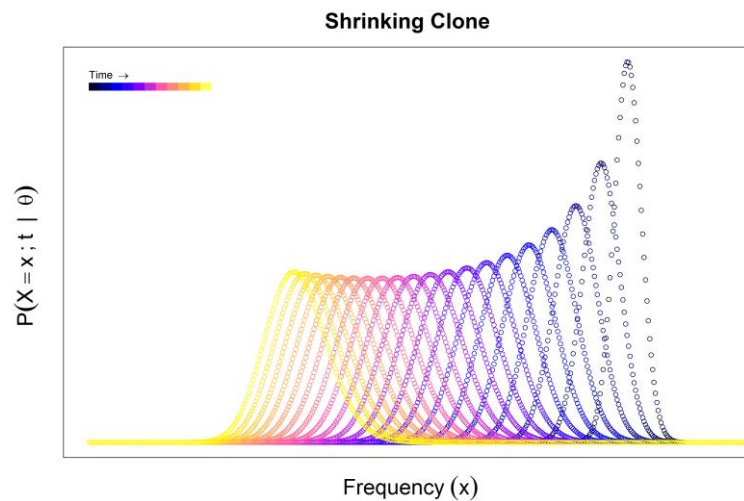


Figure 4. Probability distribution evolution. Each curve shows the distribution $\mathbb{P}(X_i; t) = \mathbb{P}(X_i(t) = x_i | X_i(0) = x_{i,0})$ of the probability that the given clone i contains x_i cells at time t . At successive time points the curve broadens and either **(A)** shifts to the right as the expected frequency of the clone increases, or **(B)** shifts to the left as the expected frequency of the clone decreases.

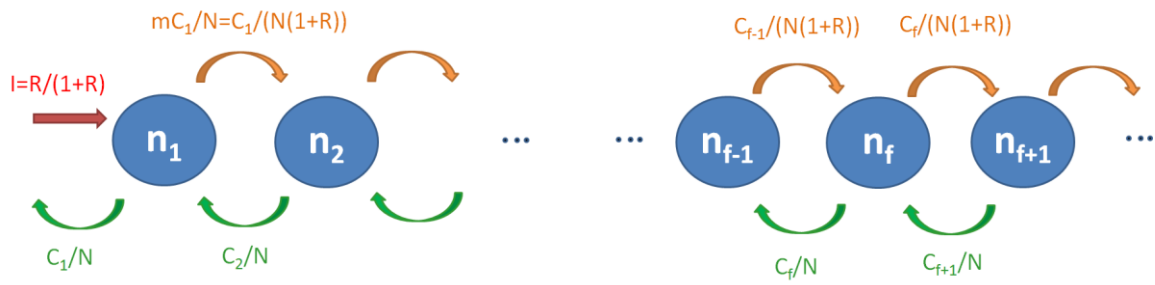


Figure 5. Occupancy class model schematic. Singletons (clones of size 1) are produced by infectious spread (red). Proliferation (orange) results in loss from clone size class f and entry into size class $f + 1$. Death of a cell (green) results in a clone moving from size class f to size class $f - 1$.

714

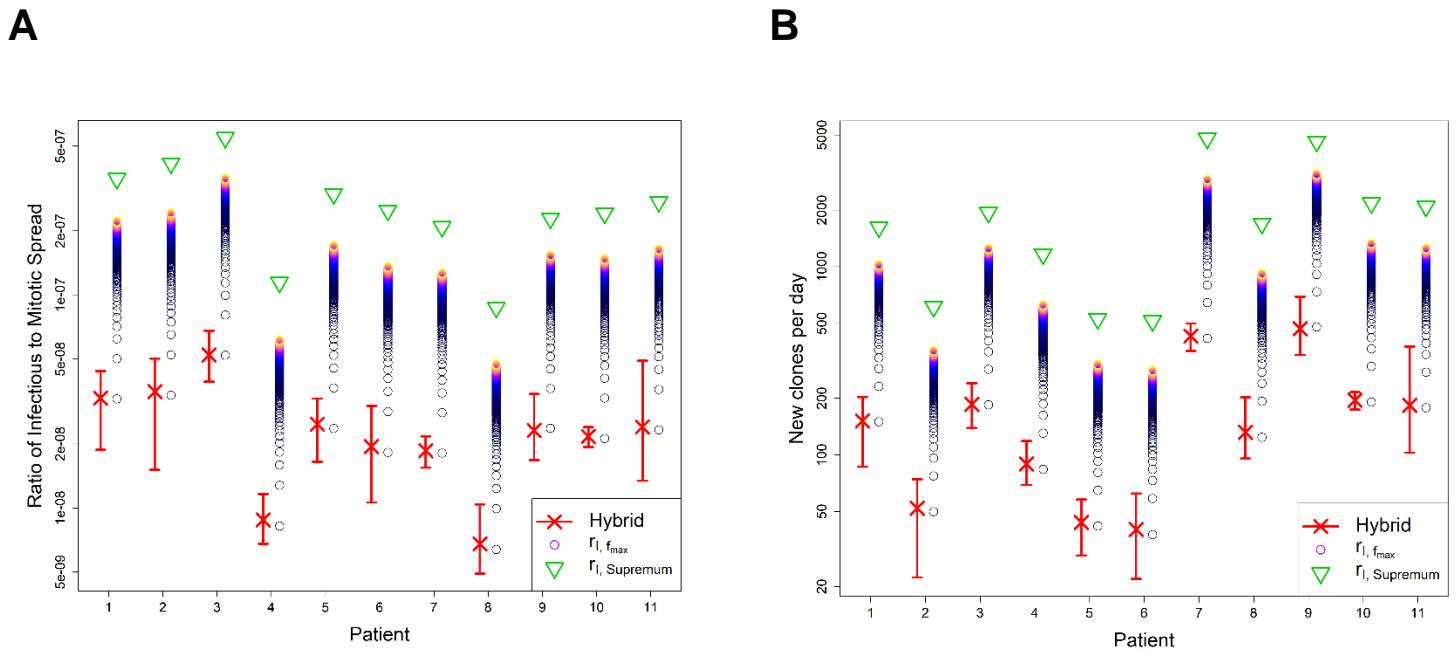


Figure 6. Ratio of infectious spread to mitotic spread and number of new clones per day, by patient and estimator. A Ratio of infectious spread to mitotic spread. **B** Number of new clones generated per day. In each plot, red crosses and bars respectively denote point estimates and the range from the nine estimates for each subject from the hybrid model. Upper bound approximations from $r_{I, Supremum}$ (green triangles) are shown, together with tighter upper bounds from $r_{I, f_{max}}$ (coloured circles) for multiple values of f_{max} between 1 and 1000. Lighter colours denote higher values of f_{max} . Hybrid model point estimates are very close to the estimates obtained for $f_{max} = 1$ (lowest circles). Estimates plotted on logarithmic scale.

715

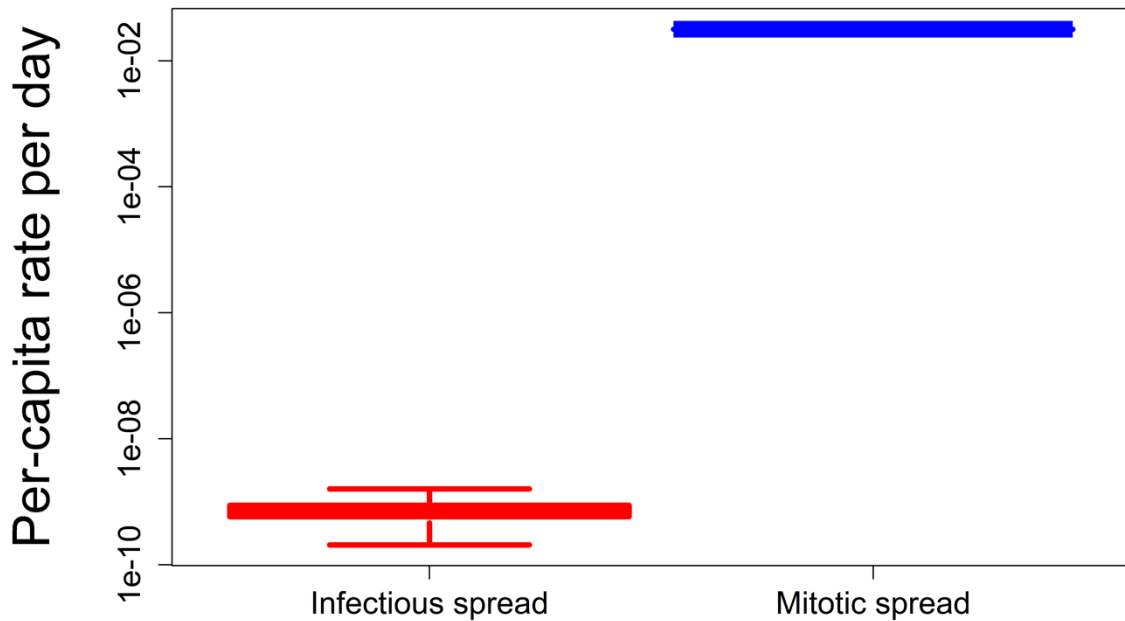


Figure 7. Infectious and mitotic spread rates. Per-capita rates of infectious spread (using hybrid model) and mitotic spread are shown. Infectious spread rates are fitted to HTLV-1 clonal diversity estimates from 11 patients. Mitotic spread rates are derived from previously obtained values [supplementary information]. Mitotic spread is substantially higher than infectious spread in chronic phase of infection.

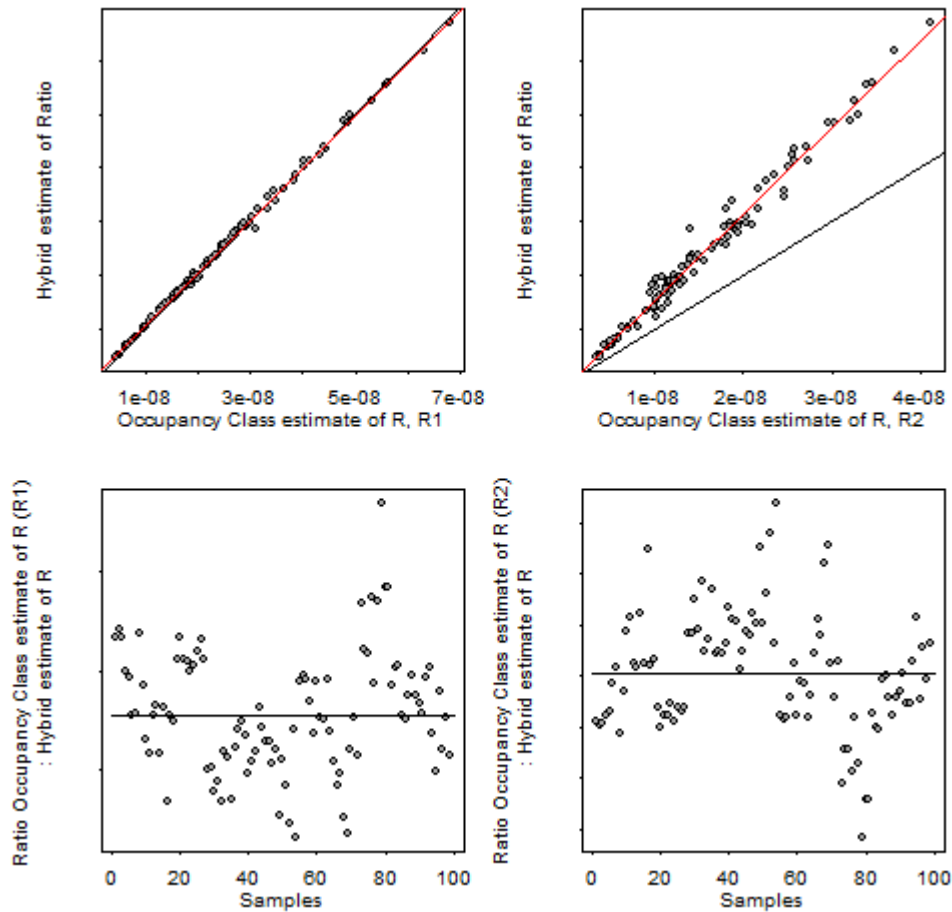


Figure 8. Comparison of estimates of ratio of infectious to mitotic spread from the hybrid model (method 1) and the occupancy class model (method 3). (Top left) Estimate of ratio from hybrid model plotted against first estimate from occupancy class model (R_1). Red line is line of best fit, black line is line of equality. (Top right) Estimate of ratio from hybrid model plotted against second estimate from occupancy class model (R_2). Red line is line of best fit, black line is line of equality. (Bottom left) Estimate of ratio between hybrid model and first estimate from occupancy class model (R_1). Black line denotes the median. (Bottom right) Estimate of ratio between hybrid model and second estimate from occupancy class model (R_2). Black line denotes the median.

717

718

719

Tables

720 **Table 1.** Hybrid model estimates of rate of infectious spread estimates and ratio of
 721 infectious to mitotic spread by patient.

Patient (Disease Status [‡])	Mean Proviral load* (no. HTLV-1+ cells per 10,000 PBMCs) [9]	Mean Estimated* diversity (no. HTLV-1+ clones in body) [10]	Infectious spread rate r_i [Mean (Lower – Upper) [†] , standard deviation within patient replicate samples]	Ratio of infectious to mitotic spread [Mean (Lower – Upper) [†] , standard deviation within patient replicate samples]	Number new clones per day [Mean (Lower – Upper) [†]]
1 (AC)	417	50666	1.0e-09 (5.9e-10 - 1.4e-09), 2.6e-10	3.3e-08 (1.9e-08 - 4.4e-08), 8.3e-9	149 (101 - 191)
2 (UV)	133	19025	1.1e-09 (4.8e-10 - 1.6e-09), 3.5e-10	3.5e-08 (1.5e-08 - 5.0e-08), 1.1e-8	51 (25 - 67)
3 (HAM)	320	59908	1.7e-09 (1.2e-09 - 2.1e-09), 3.0e-10	5.2e-08 (3.9e-08 - 6.8e-08), 9.6e-9	181 (130 - 243)
4 (HAM)	920	36840	2.8e-10 (2.1e-10 - 3.7e-10), 5.4e-11	8.8e-09 (6.8e-09 - 1.2e-08), 1.7e-9	89 (68 - 113)
5 (HAM)	160	16485	7.8e-10 (5.2e-10 - 1.0e-09), 1.9e-10	2.5e-08 (1.6e-08 - 3.3e-08), 6.0e-9	43 (33 - 58)
6 (HAM)	187	15906	6.1e-10 (3.4e-10 - 9.5e-10), 2.3e-10	1.9e-08 (1.1e-08 - 3.0e-08), 7.3e-9	39 (19 - 57)
7 (HAM)	2077	152180	5.9e-10 (4.9e-10 - 6.8e-10), 6.7e-11	1.9e-08 (1.5e-08 - 2.2e-08), 2.1e-9	428 (346 - 496)
8 (HAM)	1753	52246	2.1e-10 (1.6e-10 - 3.3e-10), 5.9e-11	6.8e-09 (4.9e-09 - 1.0e-08), 1.9e-9	128 (82 - 178)
9 (HAM)	1827	142032	7.3e-10 (5.3e-10 - 1.1e-09), 2.2e-10	2.3e-08 (1.7e-08 - 3.4e-08), 6.9e-9	456 (303 - 671)
10 (HAM)	813	68897	6.8e-10 (6.1e-10 - 7.6e-10), 6.4e-11	2.2e-08 (1.9e-08 - 2.4e-08), 2.0e-9	196 (157 - 249)
11 (HAM)	690	59145	7.6e-10 (4.2e-10 - 1.6e-09), 4.1e-10	2.4e-08 (1.3e-08 - 4.9e-08), 1.3e-8	161 (118 - 234)
Mean	845	61212	7.7e-10	2.4e-8	175

* Mean value of nine replicate samples for each patient (see methods)

[†] Lower and Upper denote the range of estimates from nine hybrid model fits from each subject.

[‡] Disease status: AC = asymptomatic carrier. UV = uveitis (non-HAM/TSP); HAM = HAM/TSP

722

723 **Table 2.** Parameter names and values

Parameter Name	Description	Comments	Value
r_I	per-capita rate of infectious spread (de novo infection)	Fitted for each patient [Methods]	See Table 1
π	per-capita rate of mitotic spread (infected cell proliferation)	Derived from [48] (supplementary information)	0.0316 per day
δ	per-capita rate of infected cell death	Derived from [48] (supplementary information)	0.0316 per day
K	Density dependency parameter. Infected cell proliferation rates are half maximal when number of infected cells $N(t) = K$	Derived from [48] (supplementary information)	4.02×10^{11}
R	Ratio of infectious to mitotic spread	derived from value of π and fitted values of r_I	See Table 1

724

725

References

726

727 1. Gessain A, Cassar O. Epidemiological Aspects and World Distribution of HTLV-
728 1 Infection. *Frontiers in microbiology*. 2012;3:388. Epub 2012/11/20. doi:
729 10.3389/fmicb.2012.00388. PubMed PMID: 23162541; PubMed Central PMCID:
730 PMC3498738.

731 2. Ishitsuka K, Tamura K. Human T-cell leukaemia virus type I and adult T-cell
732 leukaemia-lymphoma. *Lancet Oncology*. 2014;15:e517-e26.

733 3. Bangham CR, Araujo A, Yamano Y, Taylor GP. HTLV-1-associated
734 myelopathy/tropical spastic paraparesis. *Nat Rev Dis Primers*. 2015;1:15012. doi:
735 10.1038/nrdp.2015.12. PubMed PMID: 27188208.

736 4. Demontis MA, Hilburn S, Taylor GP. Human T cell lymphotropic virus type 1
737 viral load variability and long-term trends in asymptomatic carriers and in patients with
738 human T cell lymphotropic virus type 1-related diseases. *ARHR*. 2013;29(2):359-64.
739 Epub 2012/08/17. doi: 10.1089/AID.2012.0132. PubMed PMID: 22894552.

740 5. Matsuzaki T, Nakagawa M, Nagai M, Usuku K, Higuchi I, Arimura K, et al.
741 HTLV-I proviral load correlates with progression of motor disability in HAM/TSP:
742 analysis of 239 HAM/TSP patients including 64 patients followed up for 10 years.
743 *Journal of neurovirology*. 2001;7(3):228-34. PubMed PMID: 11517397.

744 6. Nagai M, Usuku K, Matsumoto W, Kodama D, Takenouchi N, Moritoyo T, et al.
745 Analysis of HTLV-I proviral load in 202 HAM/TSP patients and 243 asymptomatic

- 746 HTLV-I carriers: high proviral load strongly predisposes to HAM/TSP. *J Neurovirol.*
747 1998;4(6):586-93. Epub 1999/03/05. PubMed PMID: 10065900.
- 748 7. Okayama A, Stuver S, Matsuoka M, Ishizaki J, Tanaka G, Kubuki Y, et al. Role
749 of HTLV-1 proviral DNA load and clonality in the development of adult T-cell
750 leukemia/lymphoma in asymptomatic carriers. *Int J Cancer.* 2004;110(4):621-5. Epub
751 2004/05/04. doi: 10.1002/ijc.20144. PubMed PMID: 15122598.
- 752 8. Overbaugh J, Bangham CR. Selection forces and constraints on retroviral
753 sequence variation. *Science.* 2001;292(5519):1106-9. Epub 2001/05/16. PubMed
754 PMID: 11352065.
- 755 9. Gillet NA, Malani N, Melamed A, Gormley N, Carter R, Bentley D, et al. The
756 host genomic environment of the provirus determines the abundance of HTLV-1-
757 infected T-cell clones. *Blood.* 2011;117(11):3113-22. Epub 2011/01/14. doi: blood-
758 2010-10-312926 [pii]
759 10.1182/blood-2010-10-312926. PubMed PMID: 21228324; PubMed Central PMCID:
760 PMC3062313.
- 761 10. Laydon DJ, Melamed A, Sim A, Gillet NA, Sim K, Darko S, et al. Quantification
762 of HTLV-1 clonality and TCR diversity. *PLoS computational biology.*
763 2014;10(6):e1003646. doi: 10.1371/journal.pcbi.1003646. PubMed PMID: 24945836;
764 PubMed Central PMCID: PMC4063693.
- 765 11. Wattel E, Vartanian JP, Pannetier C, Wain-Hobson S. Clonal expansion of
766 human T-cell leukemia virus type I-infected cells in asymptomatic and symptomatic
767 carriers without malignancy. *J Virol.* 1995;69(5):2863-8. Epub 1995/05/01. PubMed
768 PMID: 7707509; PubMed Central PMCID: PMC188982.

- 769 12. Tanaka G, Okayama A, Watanabe T, Aizawa S, Stuver S, Mueller N, et al. The
770 clonal expansion of human T lymphotropic virus type 1-infected T cells: a comparison
771 between seroconverters and long-term carriers. *J Infect Dis.* 2005;191(7):1140-7.
772 Epub 2005/03/05. doi: JID33135 [pii]
773 10.1086/428625. PubMed PMID: 15747250.
- 774 13. Wattel E, Cavrois M, Gessain A, Wain-Hobson S. Clonal expansion of infected
775 cells: a way of life for HTLV-I. *J Acquir Immune Defic Syndr Hum Retrovirol.* 1996;13
776 Suppl 1:S92-9. Epub 1996/01/01. PubMed PMID: 8797710.
- 777 14. Wodarz D, Nowak MA, Bangham CR. The dynamics of HTLV-I and the CTL
778 response. *Immunol Today.* 1999;20(5):220-7. Epub 1999/05/14. doi:
779 S0167569999014462 [pii]. PubMed PMID: 10322301.
- 780 15. Berry CC, Gillet NA, Melamed A, Gormley N, Bangham CR, Bushman FD.
781 Estimating abundances of retroviral insertion sites from DNA fragment length data.
782 *Bioinformatics.* 2012;28(6):755-62. Epub 2012/01/13. doi: bts004 [pii]
783 10.1093/bioinformatics/bts004. PubMed PMID: 22238265; PubMed Central PMCID:
784 PMC3307109.
- 785 16. Cavrois M, Wain-Hobson S, Gessain A, Plumelle Y, Wattel E. Adult T-cell
786 leukemia/lymphoma on a background of clonally expanding human T-cell leukemia
787 virus type-1-positive cells. *Blood.* 1996;88(12):4646-50. Epub 1996/12/15. PubMed
788 PMID: 8977257.
- 789 17. Furukawa Y, Fujisawa J, Osame M, Toita M, Sonoda S, Kubota R, et al.
790 Frequent clonal proliferation of human T-cell leukemia virus type 1 (HTLV-1)-infected

- 791 T cells in HTLV-1-associated myelopathy (HAM-TSP). *Blood*. 1992;80(4):1012-6.
792 Epub 1992/08/15. PubMed PMID: 1498321.
- 793 18. Gabet AS, Mortreux F, Talarmin A, Plumelle Y, Leclercq I, Leroy A, et al. High
794 circulating proviral load with oligoclonal expansion of HTLV-1 bearing T cells in HTLV-
795 1 carriers with strongyloidiasis. *Oncogene*. 2000;19(43):4954-60. Epub 2000/10/24.
796 doi: 10.1038/sj.onc.1203870. PubMed PMID: 11042682.
- 797 19. Meekings KN, Leipzig J, Bushman FD, Taylor GP, Bangham CR. HTLV-1
798 integration into transcriptionally active genomic regions is associated with proviral
799 expression and with HAM/TSP. *PLoS Pathog*. 2008;4(3):e1000027. Epub 2008/03/29.
800 doi: 10.1371/journal.ppat.1000027. PubMed PMID: 18369476; PubMed Central
801 PMCID: PMC2265437.
- 802 20. Bangham CR. Human T-cell leukaemia virus type I and neurological disease.
803 *Curr Opin Neurobiol*. 1993;3(5):773-8. Epub 1993/10/01. PubMed PMID: 8260828.
- 804 21. Cook LB, Melamed A, Niederer H, Valganon M, Laydon D, Foroni L, et al. The
805 role of HTLV-1 clonality, proviral structure, and genomic integration site in adult T-cell
806 leukemia/lymphoma. *Blood*. 2014;123(25):3925-31. doi: 10.1182/blood-2014-02-
807 553602. PubMed PMID: 24735963; PubMed Central PMCID: PMC4064332.
- 808 22. Gillet NA, Cook L, Laydon DJ, Hlela C, Verdonck K, Alvarez C, et al.
809 Strongyloidiasis and infective dermatitis alter human T lymphotropic virus-1 clonality
810 in vivo. *PLoS Path*. 2013;9(4):e1003263. Epub 2013/04/18. doi:
811 10.1371/journal.ppat.1003263
- 812 PPATHOGENS-D-12-02814 [pii]. PubMed PMID: 23592987; PubMed Central PMCID:
813 PMC3617147.

- 814 23. Taylor GP, Hall SE, Navarrete S, Michie CA, Davis R, Witkover AD, et al. Effect
815 of lamivudine on human T-cell leukemia virus type 1 (HTLV-1) DNA copy number, T-
816 cell phenotype, and anti-tax cytotoxic T-cell frequency in patients with HTLV-1-
817 associated myelopathy. *Journal of virology*. 1999;73(12):10289-95.
- 818 24. Laydon DJ, Bangham CR, Asquith B. Estimating T-cell repertoire diversity:
819 limitations of classical estimators and a new approach. *Phil Trans R Soc Lond B*.
820 2015;370(1675). doi: 10.1098/rstb.2014.0291. PubMed PMID: 26150657; PubMed
821 Central PMCID: PMCPMC4528489.
- 822 25. Laydon DJ, Sim A, Bangham CRM, Asquith B. DivE: Diversity Estimator. 1.1
823 ed2019.
- 824 26. Jahnke T, Kreim M. Error bound for piecewise deterministic processes
825 modeling stochastic reaction systems. *Multiscale Modeling & Simulation*.
826 2012;10(4):1119-47.
- 827 27. Jahnke T, Sunkara V. Error Bound for Hybrid Models of Two-Scaled Stochastic
828 Reaction Systems. In: Dahlke S, Dahmen W, Griebel M, Hackbusch W, Ritter K,
829 Schneider R, et al., editors. *Extraction of Quantifiable Information from Complex*
830 *Systems*. Cham: Springer International Publishing; 2014. p. 303-19.
- 831 28. Gillespie DT. A rigorous derivation of the chemical master equation. *Physica A:*
832 *Statistical Mechanics and its Applications*. 1992;188(1):404-25.
- 833 29. Jahnke T. On reduced models for the chemical master equation. *Multiscale*
834 *Modeling & Simulation*. 2011;9(4):1646-76.

- 835 30. Van Kampen NG. Stochastic processes in physics and chemistry: Elsevier;
836 1992.
- 837 31. Hegland M, Burden C, Santoso L, MacNamara S, Booth H. A solver for the
838 stochastic master equation applied to gene regulatory networks. *Journal of*
839 *computational and applied mathematics*. 2007;205(2):708-24.
- 840 32. Jahnke T, Huisinga W. A dynamical low-rank approach to the chemical master
841 equation. *Bulletin of mathematical biology*. 2008;70(8):2283-302.
- 842 33. Stewart WJ. Introduction to the numerical solutions of Markov chains: Princeton
843 Univ. Press; 1994.
- 844 34. Strang G. On the construction and comparison of difference schemes. *SIAM*
845 *Journal on Numerical Analysis*. 1968;5(3):506-17.
- 846 35. Asquith B, McLean AR. In vivo CD8+ T cell control of immunodeficiency virus
847 infection in humans and macaques. *PNAS*. 2007;104(15):6365-70. Epub 2007/04/04.
848 doi: 0700666104 [pii]
- 849 10.1073/pnas.0700666104. PubMed PMID: 17404226.
- 850 36. Chao A. Nonparametric estimation of the number of classes in a population.
851 *Scandinavian Journal of Statistics*. 1984;11(4):265-70.
- 852 37. La Gruta NL, Rothwell WT, Cukalac T, Swan NG, Valkenburg SA, Kedzierska
853 K, et al. Primary CTL response magnitude in mice is determined by the extent of naive
854 T cell recruitment and subsequent clonal expansion. *The Journal of Clinical*
855 *Investigation*. 2010;120(6):1885-94.

- 856 38. Gwinn DC, Allen MS, Bonvechio KI, V. Hoyer M, Beesley LS. Evaluating
857 estimators of species richness: the importance of considering statistical error rates.
858 *Methods in Ecology and Evolution*. 2016;7(3):294-302.
- 859 39. Hamad I, Ranque S, Azhar EI, Yasir M, Jiman-Fatani AA, Tissot-Dupont H, et
860 al. Culturomics and amplicon-based metagenomic approaches for the study of fungal
861 population in human gut microbiota. *Scientific reports*. 2017;7(1):16788.
- 862 40. Branco M, Figueiras FG, Cermeño P. Assessing the efficiency of non-
863 parametric estimators of species richness for marine microplankton. *Journal of*
864 *Plankton Research*. 2018;40(3):230-43.
- 865 41. R Core Team. R: A language and environment for statistical computing
866 [Internet]. Vienna, Austria; 2018. 3.5.0 ed. Vienna, Austria: R Foundation for Statistical
867 Computing; 2018.
- 868 42. Dowle M, Srinivasan A, Gorecki J, Short T, Lianoglou S, Antonyan E. data.
869 table: extension of data. frame. R package version 1.9. 8. 2016. 2017.
- 870 43. Bates D, Maechler M, Maechler MM. Package 'Matrix'. 2017.
- 871 44. Arioli M, Codenotti B, Fassino C. The Padé method for computing the matrix
872 exponential. *Linear algebra and its applications*. 1996;240:111-30.
- 873 45. Brent RP. Algorithms for minimization without derivatives: Courier Corporation;
874 2013.
- 875 46. de Greef PC, Oakes T, Gerritsen B, Ismail M, Heather JM, Hermsen R, et al.
876 The naive T-cell receptor repertoire has an extremely broad distribution of clone sizes.
877 *bioRxiv*. 2019:691501. doi: 10.1101/691501.

878 47. Niederer HA, Laydon DJ, Melamed A, Elemans M, Asquith B, Matsuoka M, et
879 al. HTLV-1 proviral integration sites differ between asymptomatic carriers and patients
880 with HAM/TSP. *Virology journal*. 2014;11(1):172.

881 48. Asquith B, Zhang Y, Mosley AJ, de Lara CM, Wallace DL, Worth A, et al. In vivo
882 T lymphocyte dynamics in humans and the impact of human T-lymphotropic virus 1
883 infection. *Proc Natl Acad Sci U S A*. 2007;104(19):8035-40. Epub 2007/05/08. doi:
884 0608832104 [pii]

885 10.1073/pnas.0608832104. PubMed PMID: 17483473; PubMed Central PMCID:
886 PMC1861853.

887